Materials Today Bio 28 (2024) 101212

Contents lists available at ScienceDirect

Materials Today Bio

journal homepage: www.journals.elsevier.com/materials-today-bio

Tough and self-adhesive zwitterionic hydrogels with mechano-responsive release of bFGF for tympanic membrane repair

Shengjia Chen [a,b,c,d], Xiangshu Guo [b,c], Yanyu Yang [b,c], Junjie Deng [b,c], Ting Xu [b,c], Zhechen Yuan [d], Hao Xue [a], Longxing Niu [b,c,**], Rong Wang [b,c,*], Yi Shen [a,d,***]

[a] Department of Otorhinolaryngology Head and Neck Surgery, The Affiliated Lihuili Hospital of Ningbo University, Ningbo, 315040, Zhejiang, PR China
[b] Laboratory of Advanced Theranostic Materials and Technology, Ningbo Institute of Materials Technology and Engineering, Chinese Academy of Sciences, Ningbo, 315201, PR China
[c] Zhejiang International Scientific and Technological Cooperative Base of Biomedical Materials and Technology, Ningbo Cixi Institute of Biomedical Engineering, Ningbo, 315300, PR China
[d] School of Medicine, Ningbo University, Ningbo, 315211, PR China

ARTICLE INFO

Keywords:
Tympanic membrane perforation
Basic fibroblast growth factor
Hydrogels
Mechano-responsive release
Vibration

ABSTRACT

The tympanic membrane (TM) is constantly in a state of vibrating. However, there is currently a lack of drug-delivery scaffolds suitable for the dynamic environment of TM perforation. In this study, a mechano-responsive tough hydrogel was developed. It consists of basic fibroblast growth factor (bFGF)-loaded sodium alginate (SA) microspheres, polysulfobetaine methacrylate (polySBMA), and gelatin methacrylate (GelMA). This hydrogel was designed to serve as a TM scaffold to promote perforation healing under dynamic conditions. bFGF was encapsulated in SA microspheres, which were then incorporated into polySBMA-GelMA hydrogels through photo-initiated free radical polymerization. The mechanical properties, tissue adhesiveness, swelling properties, and degradation of the hydrogels were evaluated before and after microsphere incorporation. It was observed that incorporating bFGF-loaded SA microspheres did not significantly impact the adhesion and degradation mechanisms of the hydrogel. The compressive strength and tensile strength of the microsphere-incorporated hydrogel were up to 6.6 MPa and 64.1 kPa, respectively, suitable for a TM scaffold. The release behavior of bFGF from the hydrogel could be controlled by vibration stimulation without significantly affecting the hydrogel's mechanical properties, indicating a mechano-responsive nature of the hydrogel. The *in vitro* cytotoxicity assay demonstrated that the hydrogels showed no cytotoxic effects. Moreover, cell culture assays demonstrated that vibration stimulation could enhance the release of bFGF, significantly promoting cell proliferation and migration. The results demonstrate the significant potential of the mechano-responsive hydrogel as a scaffold for repairing TM perforations.

1. Introduction

Tympanic membrane (TM) perforation is a widespread clinical challenge [1,2]. In specific groups such as Indigenous Australians, the reported prevalence has been as high as 28–43 % [3]. If the acute perforation is not promptly closed, it will progress to chronic perforation [4,5], which can lead to recurrent episodes of otitis media, hearing loss, and severe headaches [6]. The acute TM perforation can heal spontaneously within 6–8 weeks. However, the chronic TM perforation needs to be repaired through surgery to improve hearing and reduce the frequency of otitis media. Myringoplasty is a common therapeutic procedure where autogenous materials such as temporal muscle fascia, tragus cartilage, fat, and perichondrium act as scaffolds for regenerating TM tissue [7,8]. However, this treatment is usually limited by the shortage of available tissues, multiple postoperative complications, and high operating costs. It is an urgent challenge to explore artificial materials due to the advancement of ear endoscopy technology and the increasing need for minimally invasive surgery for both doctors and

* Corresponding author.
** Corresponding author.
*** Corresponding author. Department of Otorhinolaryngology Head and Neck Surgery, The Affiliated Lihuili Hospital of Ningbo University, Ningbo, 315040, Zhejiang, PR China.
E-mail addresses: niulongxing@nimte.ac.cn (L. Niu), rong.wang@nimte.ac.cn (R. Wang), tyzdhs@163.com (Y. Shen).

https://doi.org/10.1016/j.mtbio.2024.101212
Received 20 April 2024; Received in revised form 14 August 2024; Accepted 23 August 2024
Available online 24 August 2024

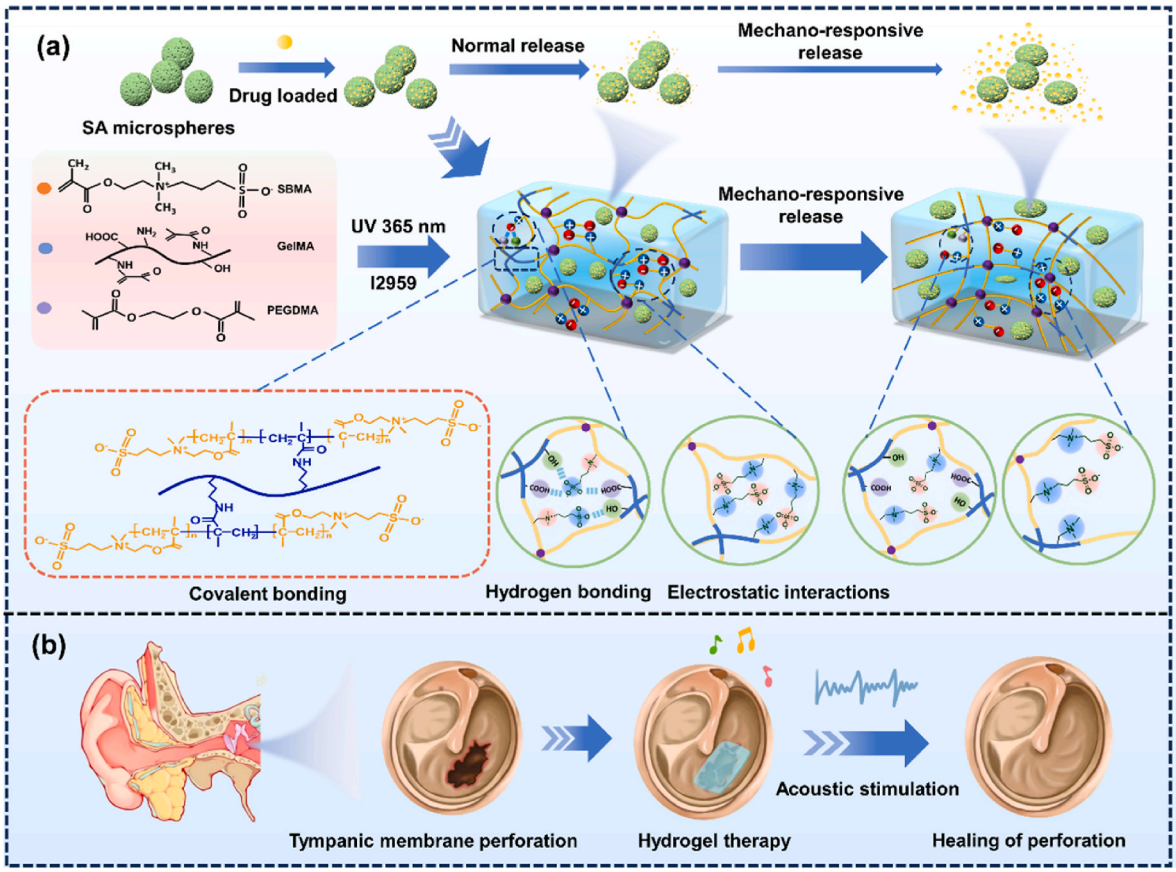

Fig. 1. Schematic illustration of (a) the process of preparing SG_xM_y hydrogels and the mechano-responsive release of drugs upon hydrogel deformation, and (b) the application of mechano-responsive hydrogel for the treatment of TM perforation.

patients.

Basic fibroblast growth factor (bFGF) has been demonstrated to facilitate the regeneration of TM through various mechanisms [3,4,9], including promoting the proliferation and migration of epithelial cells and fibroblasts [10]. Additionally, bFGF possesses vasodilatory properties, which are conducive to increasing local blood flow and promoting the healing of TM perforation [11]. More importantly, it exhibits preventive and restorative effects on hearing damage [10]. However, the application of bFGF in TM perforation is constrained by its short half-life, poor stability [12], and high dosage inhibiting collagen deposition [13]. To overcome these limitations, it is imperative to develop a material capable of encapsulating bFGF for precise delivery and controlled release. This will prolong the action time of growth factors in treating TM perforation.

It has been reported that moist perforation margins aid in regenerating TM perforation [14]. Hydrogels are water-swollen networks that mimic the natural tissue environment and have shown promise in TM regeneration by offering structural support at the defect site [15,16], extending drug retention time at the perforation site [17], and regulating drug release at the administration site [18]. For instance, Wang et al. [15] developed a composite hydrogel of methacryloyl hyaluronic acid/methacryloyl gelatin (GelMA), and extracellular cartilage matrix. This hydrogel could promote TM perforation healing within a week and complete TM repair within 2 months without affecting its function. Chitosan/lactic acid/fibrinogen injectable hydrogel loaded with growth factors significantly improved TM perforation healing rates [17]. However, most studies on TM perforation have focused on treatment in static environments. In the real scenario, TM detects various frequencies of sound. Under the action of sound waves and sound pressure, it could deform and convert sound waves into vibrations. Under dynamic environments, most conventional hydrogels struggle to maintain their mechanical strength, and functional stability, and fail to adhere tightly to tissues. This limitation could impede or prolong the wound healing process, potentially resulting in chronic otorrhea, hearing loss, and increased susceptibility to infections. Considering the dynamic mechanical environment inherent to the TM, it is hypothesized that developing a hydrogel capable of releasing growth factors in response to mechanical stimulation, while also demonstrating tissue adhesion and excellent biocompatibility, will provide a novel therapeutic strategy for the clinical management of TM perforation. Currently, various mechano-responsive hydrogels that adjust their properties in response to external mechanical stimuli have been developed. Our group used Pluronic F127 diacrylate micelles loaded with hydrophobic antibacterial drugs as a macro-crosslinker to create polysulfobetaine methacrylate (polySBMA) hydrogel. This approach enabled mechanically responsive drug release, promoting the healing of acute skin wounds in areas susceptible to body movement [19]. The wearable drug delivery device developed by Di et al. [20] utilized polylactic acid-glycolic acid particles for loading adriamycin and encapsulated them in alginate microgel. The drug release was effectively stimulated by tensile strain. Despite the achievements in mechano-responsive drug delivery systems, there is still a lack of research on using such hydrogels for precise control of drug release in TM perforation repair.

Alginate is a widely used carrier for growth factors because of its unique characteristics such as biocompatibility, biodegradability, non-immunogenicity, pH sensitiveness, and mucoadhesiveness [21–23]. In addition, alginate could form microspheres or hydrogel in the presence of divalent cations, such as Ca^{2+}, which minimize the risk of peptide/-protein denaturation during the formulation process [24,25]. The alginate-based systems could also protect peptides and proteins from degradation until their release. Sodium alginate (SA) microspheres have been widely used for encapsulation of bFGF [26–28]. However, SA

microspheres face several challenges, including poor mechanical strength, adhesion issues, and inaccurate or sudden drug release. Introducing an outer hydrogel matrix can effectively compensate for the above shortcomings. Zwitterionic polymers, such as polySBMA, exhibit excellent tissue adhesion and mechanical properties [19]. Moreover, polySBMA is a preferred material for protein drug delivery systems due to its high biocompatibility and non-immunogenicity [29]. PolySBMA hydrogels have been reported to promote acute wound regeneration by enhancing angiogenesis, reducing inflammation response, and modulating macrophage polarization [30,31]. However, polySBMA-based hydrogels often face the challenge of substantial swelling and limited bioactivity [32]. As the hydrolysis product of collagen, gelatin contains arginine-glycine-aspartic acid sequences for cell attachment and the target sequences of matrix metalloproteinase for cell remodeling [33]. In addition, the introduction of methacryloyl substituent groups makes gelatin photo-crosslinkable [33–35]. Incorporating GelMA can enhance the mechanical properties, bioactivity, and tissue affinity of the hydrogels.

The present study developed a tough hydrogel using bFGF-loaded SA microspheres, polySBMA, and GelMA (Fig. 1). This hydrogel was designed to deliver bFGF in response to mechanical stimuli, aiming to address the challenge of TM perforation healing within a dynamic mechanical environment. The alginate microspheres were used as drug carriers, and the zwitterionic polySBMA hydrogels possess tissue adhesion, while the incorporation of GelMA as biocompatible crosslinkers enhances their mechanical properties and improves the biocompatibility of the hydrogel. The release of drugs from the hydrogel can be controlled by stimulating the vibration of the eardrum. The study investigated and optimized the mechanical properties, tissue adhesion properties, cytotoxicity, cell proliferation, migration properties, and most importantly, the drug release profile of the hydrogel under vibration stimulation.

2. Materials and Methods

2.1. Materials

Sodium alginate (SA, viscosity 200 ± 20 mPa s), calcium chloride, [2-(methacryloxy)ethyl]dimethyl-(3-sulfonate propyl)ammonium hydroxide (SBMA, 97 %), gelatin, and methacrylic anhydride were purchased from Aladdin Chemistry (Shanghai, China). Polyethylene glycol dimethacrylate (PEGDMA, Mn = 600 Da) and fluorescein isothiocyanate (FITC) were purchased from Macklin Biochemical (Shanghai, China). 2-Hydroxy-4'-(2-hydroxyethyl)-2-methylphenylacetone (Irgacure 2959) was purchased from Energy Chemical (Anhui, China). bFGF was purchased from Beyotime Biotechnology in Shanghai, China. 5-Chloromethylfluorescein diacetate (Green CMFDA) was purchased from MedChemExpress (United States). Rat skin fibroblasts (RS1) were purchased from BeNa Culture Collection (BNCC) in Henan, China. The human immortalized epidermal cell line (HaCaT) was purchased from the China Center for Type Culture Collection (CCTCC) in Wuhan, China. Human Umbilical Vein Endothelial Cells (HUVEC) were obtained from iCell Bioscience in Shanghai, China.

2.2. Preparation of SA microspheres

SA microspheres were fabricated using the electrostatic droplet generation technology [36]. In brief, SA was dissolved in deionized water to obtain a solution with appropriate concentrations (1–2 wt%). A 10 mL standard syringe with a blunted 22-gauge needle was mounted 10 cm above the coagulation solution containing 3 wt% $CaCl_2$, and the flow rate of the injection solution was controlled to a certain flow rate using a syringe pump (LSP01-1A, Ditron-tech, China). A positive potential was applied to the upper electrode against the plate electrode using a high voltage supply (DW-P303-1ACH2, Dongwen, China). Aqueous alginate solution was dropped into the $CaCl_2$ bath to form microspheres by rapid diffusion of calcium ions into the alginate droplet. The microspheres were hardened for 20 min, and then washed thrice with deionized water. The morphology of the microspheres was observed using polarized microscopy (PM, CX40P, SOPTOP, China), or scanning electron microscopy (SEM, regulus 8230, Hitachi, Japan) after a gradient dehydration process.

Ten milliliters of SA solution was used to dissolve 20 μL of 0.1 mg/mL bFGF or FITC-bFGF (details of the synthesis procedure are given in Supporting Information), and the mixture was stirred overnight at room temperature. The drug-loaded SA microspheres were prepared in the same manner as described above. The morphology of the microspheres was observed using a polarized microscope, an inverted fluorescence microscope (ECLIPSE Ts2R, Nikon, Japan), or an SEM after a gradient dehydration process. To determine the loading efficiency (LE) of bFGF, 22 mg of microspheres (obtained from 1 mL SA-bFGF solution) were dissolved in 1 mL of 3 wt% sodium citrate solution at room temperature for 24 h, centrifugated at 10,000 rpm for 10 min, and the concentration of the released bFGF in the supernatant solution (Ct, in μg/mL) was quantified using an ELISA kit (Cusabio, China) as per the manufacturer's instruction. The LE was calculated following Equation (1):

$$LE(\%) = \frac{Ct}{0.2} \times 100\% \quad (1)$$

2.3. Hydrogel preparation

A specific quantity of GelMA (the synthesis procedure is detailed in the Supporting Information) was added to 2 mL of SBMA solution (1.4 g/mL) and then combined with PEGDMA (2.8 mg, 0.14 wt%) and Irgacure 2959 (15 mg, 0.75 wt%). After thoroughly mixing, the precursor solution was injected into a glass mold and exposed to an ultraviolet light source at a wavelength of 365 nm for 10 min. This process resulted in the formation of the hydrogel, denoted as SG_x, where S stands for SBMA, G stands for GelMA, and x represents the ratio of GelMA mass to SBMA solution volume (m/v). The chemical structure of SG_x hydrogel was analyzed using a Fourier transform infrared spectrometer (FTIR, Nicolet iS50, Thermo Fisher, United States).

For the preparation of microsphere-incorporated hydrogels, a specific amount of SA microspheres (with or without bFGF) was added to the SBMA/GelMA prepolymer solution, and the microspheres were continuously agitated until they achieved uniform dispersion within the precursor. The hydrogel was prepared in the same manner as described above and denoted as SG_xM_y, where S refers to SBMA, G refers to GelMA, x refers to the ratio of GelMA mass to SBMA solution volume (m/v), M refers to the SA microspheres, and y refers to the ratio of SA microspheres mass to SBMA/GelMA prepolymer solution volume (m/v). The dispersion of the microspheres in the hydrogel with or without compression or stretching was observed using an inverted fluorescence microscope.

2.4. Mechanical properties

Hydrogels were cut into 40 mm × 2 mm × 2 mm sizes, and their tensile properties were tested using a universal testing machine (CMT-1104, SUST, China) at a crosshead speed of 20 mm/min until reaching the breaking point. For the compression test, hydrogel samples were cut into discs of 12 mm in diameter and 5 mm in thickness. They were then compressed at a crosshead speed of 10 % strain per minute at room temperature using the universal testing machine.

2.5. Tissue adhesion properties

The adhesive strength of the hydrogels on rabbit fascia tissue was evaluated using the lap-shear method (Fig. S1). Prior to testing, fresh rabbit fascia tissue was thoroughly rinsed with deionized water to remove any dirt, and then wrapped around a titanium sheet measuring 30 mm × 10 mm × 0.5 mm. The hydrogel was cut into a 10 mm × 10

mm × 1 mm piece and sandwiched between two pieces of the fascia-wrapped titanium sheet. A 100 g weight was placed on top of the hydrogel-fascia assembly for 1 h before the testing. The two ends of the assembly were secured on a universal testing machine using clamps, and the assembly was subjected to a shear rate of 10 mm/min until it reached the breaking point. The force-displacement curves of each sample were recorded. The adhesive strength was calculated by dividing the measured maximum adhesive force by the contact area of the sample (1.0 cm^2).

2.6. Swelling properties and degradation

For the swelling experiments, the hydrogel was cut into discs with a diameter of 12 mm and a thickness of 5 mm. The discs were then immersed in 5 mL of phosphate-buffered saline (PBS, 10 mM, pH 7.2 ± 0.2) at room temperature. At the predetermined time point, water on the surface of the hydrogel was removed using filter paper, and the samples were weighed. The swelling rate (Q) of each sample was calculated using Equation (2):

$$Q = \frac{W_2\text{-}W_1}{W_1} \times 100\% \quad (2)$$

where W_1 and W_2 are the weight (in gram) of hydrogel samples before and after swelling, respectively.

For the degradation tests, hydrogel samples with a diameter of 12 mm and a thickness of 5 mm were immersed in 5 mL of PBS (10 mM, pH 7.2 ± 0.2) or 3 U/mL of collagenase at 37 °C with or without vibrations at frequency of 100 Hz, 500 Hz, 1000 Hz, or 2000 Hz. At the predetermined time point, water on the hydrogel surface was removed using filter paper, and the samples were weighed. The percentage of weight remaining (W_R) of the hydrogel was calculated using Equation (3):

$$W_R = \frac{W_b}{W_a} \times 100\% \quad (3)$$

where W_a and W_b are the weight (in gram) of hydrogel samples before and after the degradation test, respectively.

2.7. Drug release from hydrogels

Hydrogels were cut into discs with a diameter of 19 mm and a thickness of 5 mm. Subsequently, the hydrogel was covered with a rabbit fascia and placed on a vertical vibration tester (MP-3000E2, Kjinrili, China) (Fig. S2a). Vibration was applied at a fixed frequency of 0, 100, 500, 1000, or 2000 Hz for 2 h, and then any fluorescence signal on the rabbit fascia due to drug release was observed using an inverted fluorescence microscope. In the context of the quantitative experiment, the hydrogel was placed in 10 mL of PBS (10 mM, pH 7.2 ± 0.2), with the vibration frequency applied as described above for prolonged periods or altered every 2 h (Fig. S2b). At each predetermined time point, 2 mL of the sample solution containing the released drug was collected and replaced with 2 mL of fresh PBS. The concentration of the released bFGF was determined using an ELISA kit. The cumulative drug release from the hydrogel under various vibration conditions was calculated by summing the drug release over a specific period. In experiments conducted to simulate sound stimulation, the hydrogel was placed on the top of a playing radio (Fig. S2c), and the bFGF released was quantified as described above.

2.8. In vitro cytotoxicity and cell proliferation assay

Rat skin fibroblasts (RS1), a human immortalized epidermal cell line (HaCaT), and human umbilical vein endothelial cells (HUVEC) were used to assess the cytotoxicity and the cytoproliferative effect of the hydrogels. Briefly, a certain amount of SG_0, SG_5, and SG_5M_5 hydrogels were incubated in 5 mL of appropriate culture medium (Dulbecco's Modified Eagle Medium (DMEM) for RS1, Minimum Essential Medium (MEM) for HaCaT, and Endothelial Cell Medium (ECM) for HUVEC, culture medium: fetal bovine serum (FBS): penicillin-streptomycin (100 ×) = 89:10:1) at 37 °C for 24 h to obtain the extract solution. In addition, SG_5M_5 hydrogel was extracted in the appropriate culture medium under a vibration at a fixed frequency of 1000 Hz for 24 h under the same condition and then filtered using a 0.22 μm sterile filter. RS1 cells and HaCaT cells were seeded at a density of 5 × 10^4 cells per well in 24-well plates, and incubated at 37 °C and 5 % CO_2. After cultured for 24 h, the medium was replaced with extract solution from each group. Cells were cultured in the complete medium as the control group. Subsequently, after incubation for another 24 h, the relative cell proliferation rate in each group was evaluated using the Cell Counting Kit-8 (CCK-8, Beyotime, China) assay.

For the proliferation assay, RS1 cells and HaCaT cells were seeded at a density of 1 × 10^4 and 3 × 10^4 cells per well, respectively (or 1.5 × 10^4 and 5 × 10^4 cells per well, respectively, for the immunofluorescence staining assay). HUVEC cells were seeded at a density of 5 × 10^4 cells per well. The cells were maintained at 37 °C in a humidified atmosphere of 5 % CO_2. After being cultured for 8 h, the medium in each well was removed (time point set as Day 0). Subsequently, the culture medium was replaced with the extracts (1 mL, 50 mg/mL) and cultured for 5 days. The extracts were replaced every two days. Cells were cultured in the complete medium as the control group. On Day 0 and then on Days 1, 3, and 5, the medium in each well was removed, and the cell viability was evaluated using the CCK-8 assay. Immunofluorescence staining was conducted on the cells after 1, 3, and 5 days of culture. The details of the staining procedure can be found in the Supporting Information. Subsequently, the cells were examined using a confocal laser scanning microscope (CLSM, TCS SP8, Leica, Germany). The cell viability was investigated by performing live/dead staining (Beyotime, China) on the cells after 5 days of culture and observing them using a CLSM.

For two-dimensional culture of cells on hydrogel surface, hydrogel (size of 10 mm in diameter and 2 mm in thickness) was placed in a 24-well plate, and HaCaT cells were seeded on the hydrogel surface at a density of 5 × 10^4 cells per well. The cells were incubated at 37 °C with 5 % CO_2 for 1, 3, and 5 days. The cell viability was investigated through live/dead staining and subsequent observation under CLSM.

For three-dimensional culture of cells embedded in hydrogel, green CMFDA-stained RS1 cells (details of the labeling procedure are provided in Supporting Information) were dispersed homogeneously in microspheres-hydrogel precursor solution at a concentration of 1.5 × 10^4 cells per mL. Subsequently, hydrogels were prepared as described above and placed in 24-well plates. The cells were cultured as described above, and the cell viability at 1, 3, and 5 days was evaluated using CLSM.

2.9. In vitro cell migration assay

RS1 cells and HaCaT cells were seeded at a density of 5 × 10^4 and 8 × 10^4 cells per well, respectively, in 24-well plates. They were supplemented with the appropriate culture medium and then incubated at 37 °C with 5 % CO_2. After 24 h, all the cells were observed under a microscope. Once the cell fusion degree reached higher than 90 %, a sterile 10 μL pipette tip was used to create a scratch on the cell layer. The cells were washed with sterile PBS to ensure the removal of the detached cells. Subsequently, 1 mL of extracts from different groups (obtained by incubating 50 mg of hydrogels in 1 mL of the appropriate culture medium (culture medium: FBS: penicillin-streptomycin (100 ×) = 97:2:1) at 37 °C for 24 h) was added to the well. Fresh culture medium supplemented with 2 % FBS was used as the control group. Cell migration was observed and photographed under a microscope at the predetermined time points (0, 12, and 24 h). ImageJ software (Version 1.54d) was used to measure the width of the scratch. The cell migration rate was calculated using Equation (4):

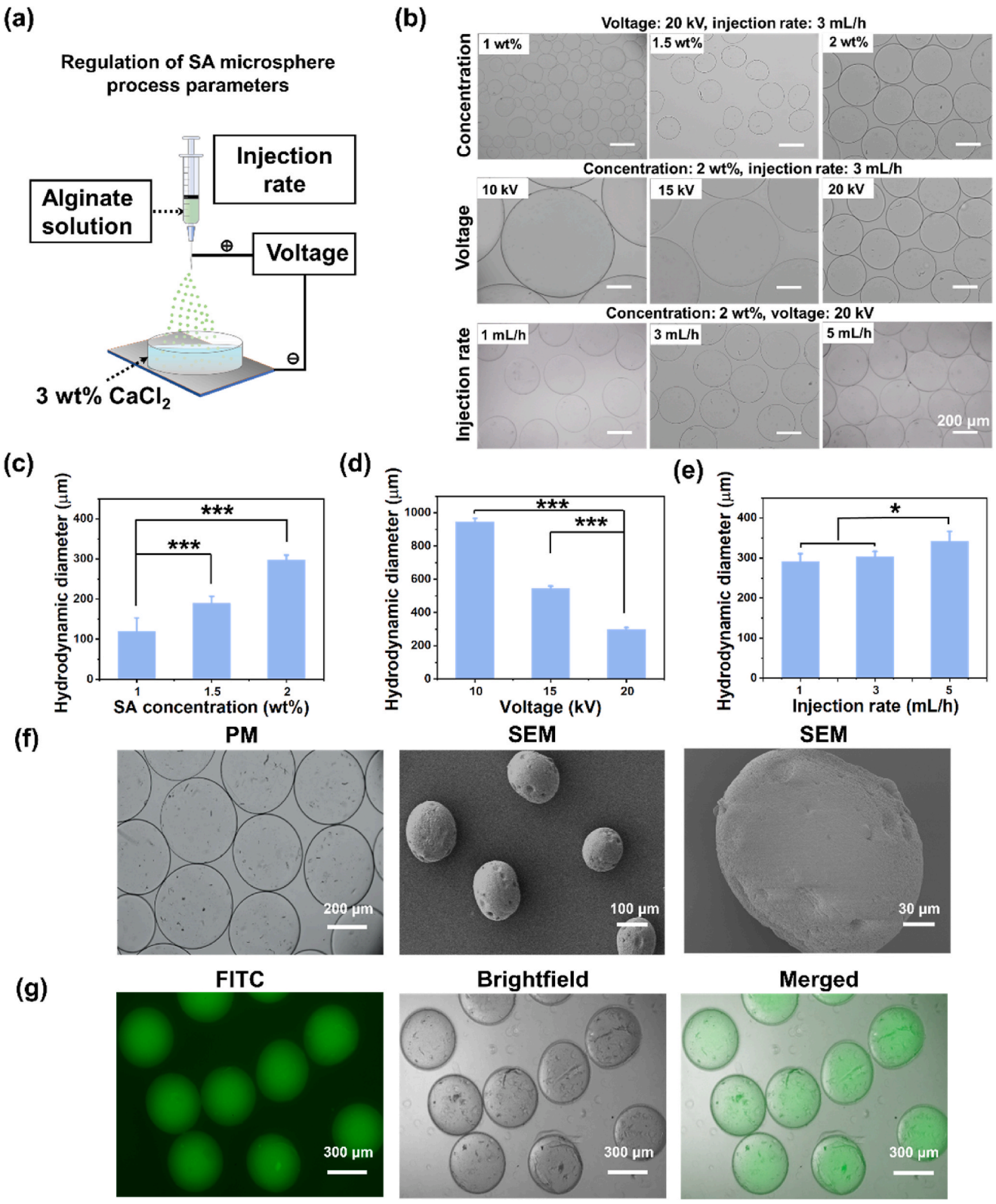

Fig. 2. Preparation and characterization of microspheres. (a) Schematic illustration of the electrostatic droplet generation technique for microsphere preparation. (b) Microscope images of SA microspheres prepared under various conditions. Hydrodynamic size of SA microspheres prepared (c) using different concentrations of SA solution with a tip voltage of 20 kV and an injection rate of 3 mL/h, (d) under different tip voltages using 2 wt% SA solution with an injection rate of 3 mL/h, and (e) with different injection rates using 2 wt% SA solution with a tip voltage of 20 kV. (f) PM and SEM images of bFGF-loaded SA microspheres prepared from 2 wt% SA solution with a tip voltage of 20 kV and an injection rate of 3 mL/h, and (g) fluorescence image of FITC-bFGF-loaded SA microspheres prepared from 2 wt% SA solution with a tip voltage of 20 kV and an injection rate of 3 mL/h.

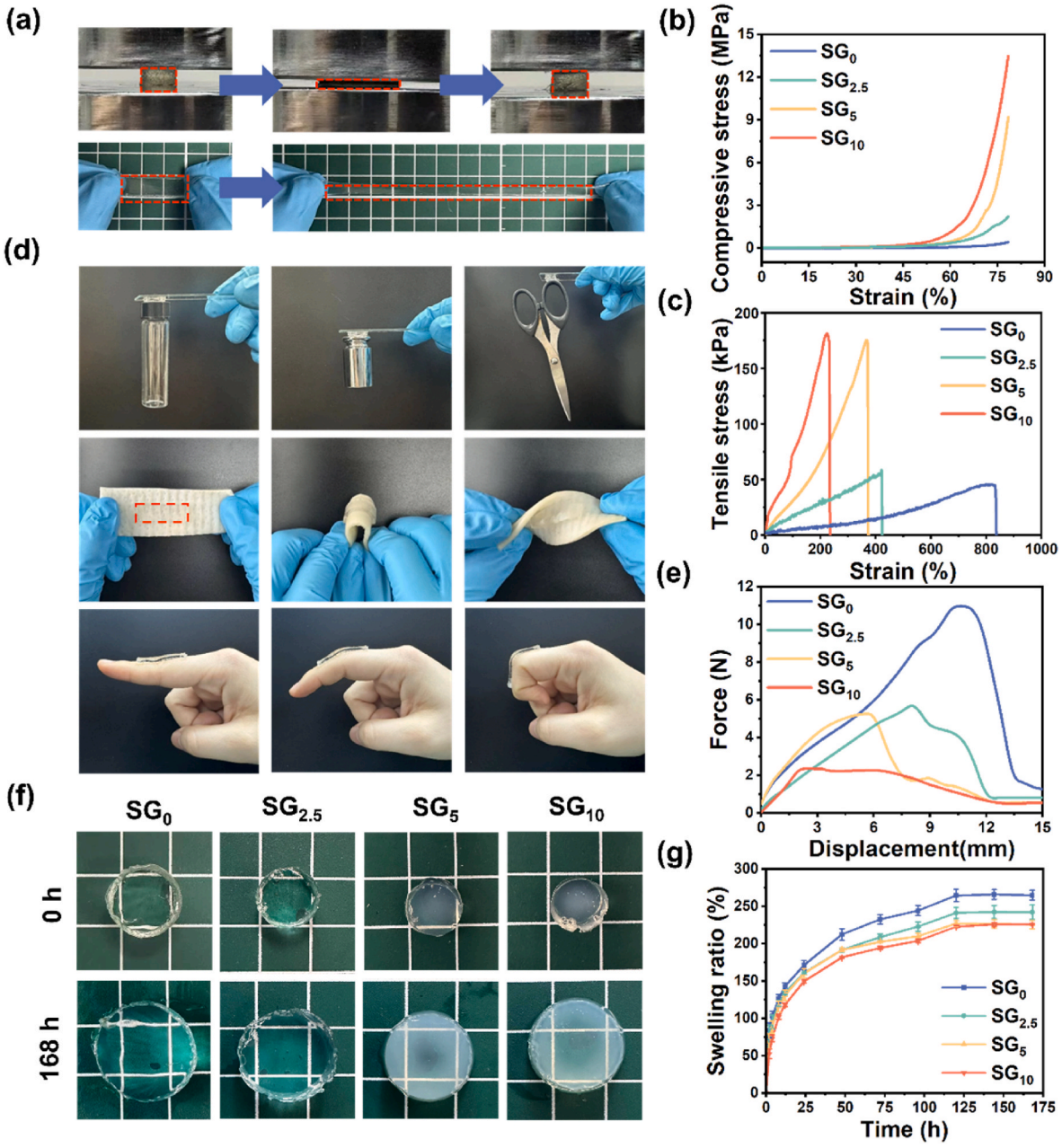

Fig. 3. (a) Representative photographs of SG_5 hydrogel demonstrate favorable self-recovery ability and stretchability. (b) Representative compressive stress-strain curves and (c) tensile stress-strain curves of SG_x hydrogels. (d) Representative photographs of SG_5 hydrogels demonstrating favorable adhesion capability on various substrate surfaces. (e) Representative adhesive force-displacement curves of SG_x hydrogels on rabbit fascia. (f) Representative photographs and (g) swelling behavior of SG_x hydrogels before and after incubation in PBS for 168 h.

$$\text{Cell migration rate } (\%) = \frac{D_0\text{-}D_x}{D_0} \times 100\% \quad (4)$$

where D_0 and D_x are the scratch width at 0 h and at the predetermined time point, respectively.

In the hydrogel surface migration assay, hydrogel discs (10 mm in diameter and 2 mm in thickness) were cut into halves and placed one half in a 24-well plate. RS1 cells and HaCaT cells were seeded on the hydrogel surface at a density of 5×10^4 and 8×10^4 cells per well, respectively. The cells were cultured as described above for 48 h. Then, the other half of the hydrogel was added, and the two pieces of hydrogel were connected with each other, forming the original disc without any interstitial gaps. The cells were further cultured for 24 h and observed using CLSM after live/dead staining.

2.10. Statistical analysis

All results presented were averaged from at least three samples for each group and reported as mean ± standard deviation. One-way analysis of variance (ANOVA) with Bonferroni post hoc test was employed to determine the statistical significance between groups. A p-value of less than 0.05 was considered statistically significant (*$p < 0.05$, **$p < 0.01$, ***$p < 0.001$).

3. Results and Discussion

3.1. Preparation of drug-loaded SA microspheres

Electrostatic droplet generation utilizes electrostatic forces to

overcome the surface tension and viscosity of the liquid, transforming large droplets into small, charged beads. The process is gentle on the bioactive substance, enabling the production of microspheres with spherical, monodisperse, and adjustable size [37–39]. Therefore, it was used to prepare SA microspheres in this study (Fig. 2a). The size and sphericity of the SA microsphere are critical for biomedical applications [39]. Small beads are more resistant to shear and compression forces, making them less likely to trigger an immune response. In addition, the mechanical and chemical stability of SA microspheres has been reported to increase with sphericity. Fractures and cracks can occur in non-spherical and tear-shaped microspheres, leading to burst release of encapsulants [40]. In this study, the size and sphericity of the microspheres were adjusted by altering the concentration of the SA solution, injection voltage, and injection rate (Fig. 2a).

Firstly, the injection voltage was fixed at 20 kV, and the injection rate was 3 mL/h. As can be seen, the hydrodynamic diameter of the microspheres gradually increased from 119.7 ± 33.4 μm to 298.4 ± 11.1 μm as the SA concentration increased from 1 wt% to 2 wt% (Fig. 2b and c). This increase is likely due to the higher solution viscosity hindering the differentiation of the droplets, resulting in an enlargement of the microsphere size [39]. Using SA solution with concentrations below 2 wt % resulted in deformation of the microspheres (Fig. 2b and S3). The viscous forces within the droplet help maintain its spherical shape, while the surrounding solution exerts drag forces on the bead surface, potentially disrupting the microspheres. Electrospray particles generated from low concentrations of SA solutions are generally unable to withstand drag forces and maintain their spherical shape upon collision with the gelling solution surface [39,40]. Generally, SA microspheres with higher sphericity exhibited greater stability (Fig. 2b and S3). However, when the concentration of SA exceeds 2 wt%, the solution becomes too viscous to pass through the needle.

Next, the concentration of the SA solution was fixed at 2 wt%, and it was injected at a rate of 3 mL/h. As the injection voltage increased from 10 kV to 20 kV, the hydrodynamic diameter of the microspheres gradually decreased from 944.0 ± 23.0 μm to 298.4 ± 11.1 μm (Fig. 2b and d). This phenomenon occurred due to the increased voltage, which generated a greater electrostatic force between the needle and the collecting substrate, causing the droplets to break into smaller microspheres during the electrospray process [41]. However, the voltage did not significantly affect the sphericity of the microspheres.

Finally, the SA solution was fixed at a concentration of 2 wt%, and the injection voltage was set to 20 kV. When the injection rate increased from 1 mL/h to 5 mL/h, the hydrodynamic size of the microspheres gradually increased from 291.8 ± 19.9 μm to 340.7 ± 25.9 μm (Fig. 2b and e). An increase in the injection rate resulted in a higher accumulation of liquid at the needle tip, leading to a rise in conical droplets suspended on the needle tip [42]. Consequently, microspheres with larger sizes were formed. It was also observed that when the injection rate was below 1 mL/h, the aggregation of conical droplets at the needle tip was too slow to produce a steady cone-jet. This resulted in heterogeneous microsphere sizes, and low sphericity of microspheres, and consequently, the microspheres were prone to collapse (Fig. S3). Notably, there was no significant difference in the size of microspheres prepared with injection rates of 1 mL/h and 3 mL/h. However, microspheres prepared at an injection rate of 3 mL/h exhibited better size uniformity and higher yields. The above results indicate that microspheres produced from a 2 wt% SA solution, using a tip voltage of 20 kV and an injection rate of 3 mL/h, exhibited good sphericity and a small and uniform size.

The drug loading performance of the microspheres and their binding to the hydrogel were further investigated. As can be seen, the hydrodynamic size of the bFGF-loaded microspheres slightly increased compared to that of pure SA microspheres (Fig. 2b and f). The fluorescence images showed that the microspheres prepared with SA solution at a concentration lower than 2 wt% could not encapsulate bFGF molecules stably, while the microspheres prepared with a voltage of 15 kV showed cracks and voids when they were incorporated in the hydrogel (Fig. S4). In contrast, the bFGF was evenly distributed in the microspheres at a concentration of 2 %, a voltage of 20 kV and a flow rate of 3 mL/h, with no noticeable phase separation between bFGF and SA (Fig. 2g), and the microspheres were able to bind tightly to the hydrogel (Fig. S4). The LE of bFGF in microspheres is calculated to be 80.3 ± 3.9 %. In summary, the microspheres prepared at an SA concentration of 2 %, a voltage of 20 kV and a flow rate of 3 mL/h were selected for the rest of the study.

3.2. Mechanical properties, tissue adhesion, and swelling properties of SG_x hydrogels

The TM is frequently subjected to acoustic wave-induced vibrations, necessitating TM repair materials with suitable mechanical strength and tissue adhesion properties. In this study, candidate hydrogels were prepared through free radical polymerization of SBMA and GelMA (with a grafting degree of 46 %, as shown in Fig. S5). As shown in Fig. S6, peaks at 1166 cm^{-1} and 1033 cm^{-1}, belonging to asymmetric and symmetrical stretching of S=O of polySBMA [43], and peak at 3435 cm^{-1}, belonging to C=O stretching vibration of gelatin [44], appeared at the SG_5 spectrum, indicating the formation of hydrogel network containing GelMA and polySBMA.

The SG_x hydrogels (SG_5 as a demonstration) exhibited excellent self-recovery capability after compression and outstanding extensibility after tension (Fig. 3a). The mechanical properties of SG_x hydrogels with varying GelMA contents were thoroughly studied (Fig. 3b and c). As the concentration of GelMA in the precursor solution increased from 0 wt% to 10 wt%, the compressive strength of the hydrogel increased significantly from 0.4 MPa to 13.4 MPa. Similarly, the tensile strength improved from 43.4 kPa for SG_0 to 180.9 kPa for SG_{10}, indicating a strong dependence of the mechanical properties of SG_x hydrogels on GelMA contents. The introduction of GelMA may increase the density of crosslinking points, resulting in a denser network structure in the hydrogel [45]. However, the fracture strains of the SG_{10} hydrogel decreased to 225 %. Excessive GelMA content may impede the migration of molecular chains, leading to a reduction in the fracture strain of the hydrogel [45].

Sufficient adhesion capability is necessary to ensure that the hydrogel remains stable on the wound site during the repair process. The TM is inclined and lacks supporting tissue beneath it [46], which makes adhesion a crucial factor in this instance. The zwitterionic SBMA groups confer the SG_x hydrogel with excellent adhesion properties through ion-dipole and dipole-dipole interactions with the surface [47]. As shown in Fig. 3d, the SG_5 hydrogel can firmly adhere to diverse surfaces, including plastic and stainless steel, as well as pig skin and fingers, even when subjected to various degrees of twisting or bending. The adhesion strength of SG_0 hydrogel to rabbit fascia was 110.7 kPa (i.e., 11.07 N, Fig. 3e). As the GelMA content in the precursor solution increased from 2.5 wt% to 10 wt%, the adhesive strength decreased from 57.4 kPa (i.e., 5.74 N) for $SG_{2.5}$–24.3 kPa (i.e., 2.43 N) for SG_{10}. The decrease in adhesive strength may be attributed to the addition of GelMA, which electrostatically interacts with the SBMA groups, reducing the number of charged groups on the hydrogel surface. This limits the available interaction sites for substance adhesion at the interface [48]. Despite this, the adhesion strength of the SG_5 hydrogel remained high at 52.8 kPa (i.e., 5.28 N) and was able to adhere to the rabbit fascial surface firmly.

Hydrogels with excessive swelling ratios may lead to issues such as increased weight and potential displacement into the ear when placed on the eardrum, resulting in irreversible effects like hearing loss and the need for surgery [49]. Therefore, as a potential material for TM perforation repair applications, it is necessary for SG_x hydrogels to possess suitable swelling properties to effectively absorb middle ear discharge (mainly consisting of serous and bloody discharge) [50,51] and maintain moist perforation margins, which aid in the regeneration of TM perforations. At present, the swelling rate of most materials used for TM

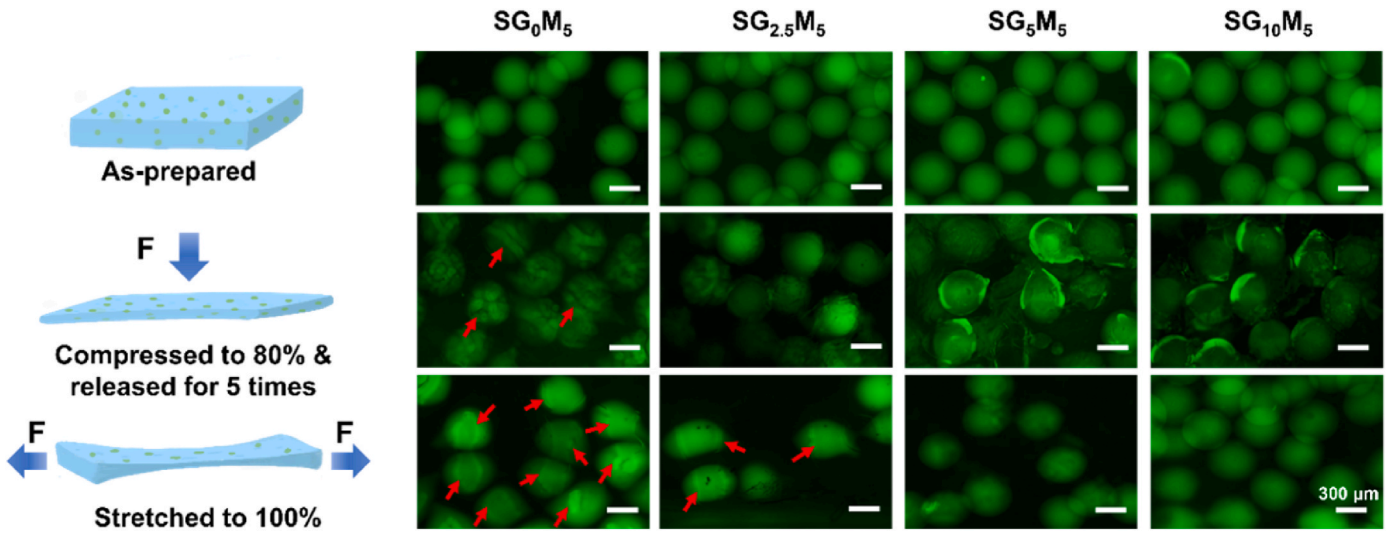

Fig. 4. Schematic illustration of the mechanical forces applied to SG_xM_5 hydrogels and representative fluorescent microscope images of SG_xM_5 hydrogels incorporated with FITC-bFGF-loaded SA microspheres after being subjected to compression or stretching. Red arrows indicate the site of hydrogel/microsphere damage or separation.

perforation repair is about 50–500 % [5,15,52]. Excessive absorption of normal tissue fluid should be avoided to prevent interference with the healing of the perforation. The swelling behavior of the SG_x hydrogels after incubation in PBS for 7 days was investigated (Fig. 3f and g). The zwitterionic SBMA groups bind water molecules through the solvation effect, resulting in a significant amount of water being contained in the hydrogel networks [53]. Therefore, the weight of SG_x hydrogels increased rapidly within 24 h and then stabilized until 120 h. The SG_0 hydrogel showed a swelling rate of around 265 %. The swelling ratio of the hydrogels was reduced to approximately 242 % after incorporating 2.5 wt% GelMA, suggesting that GelMA may enhance the stability of the hydrogels through intra/intermolecular interactions. When the GelMA content increased to 5 wt%, the swelling behavior of the hydrogel was further reduced to 226 %, likely due to the denser internal networks. However, SG_{10} hydrogels exhibited a similar swelling ratio to SG_5, suggesting that the hydrogel's stability was nearly maximized with the incorporation of 5 wt% GelMA. In general, the swelling rates of SG_x hydrogels are about 220–260 %, which is comparable to that of the reported alginate hydrogel-polycaprolactone/gelatin nanofibers composite scaffold (257.2 ± 10.3 %) [49] and polylactic acid/SA scaffolds (~250 %) [5], indicating the suitability of the swelling rate of SG_x hydrogel developed in this work.

In addition, the SBMA groups adsorb water molecules through electrostatic interactions, increase the saturated water content, and

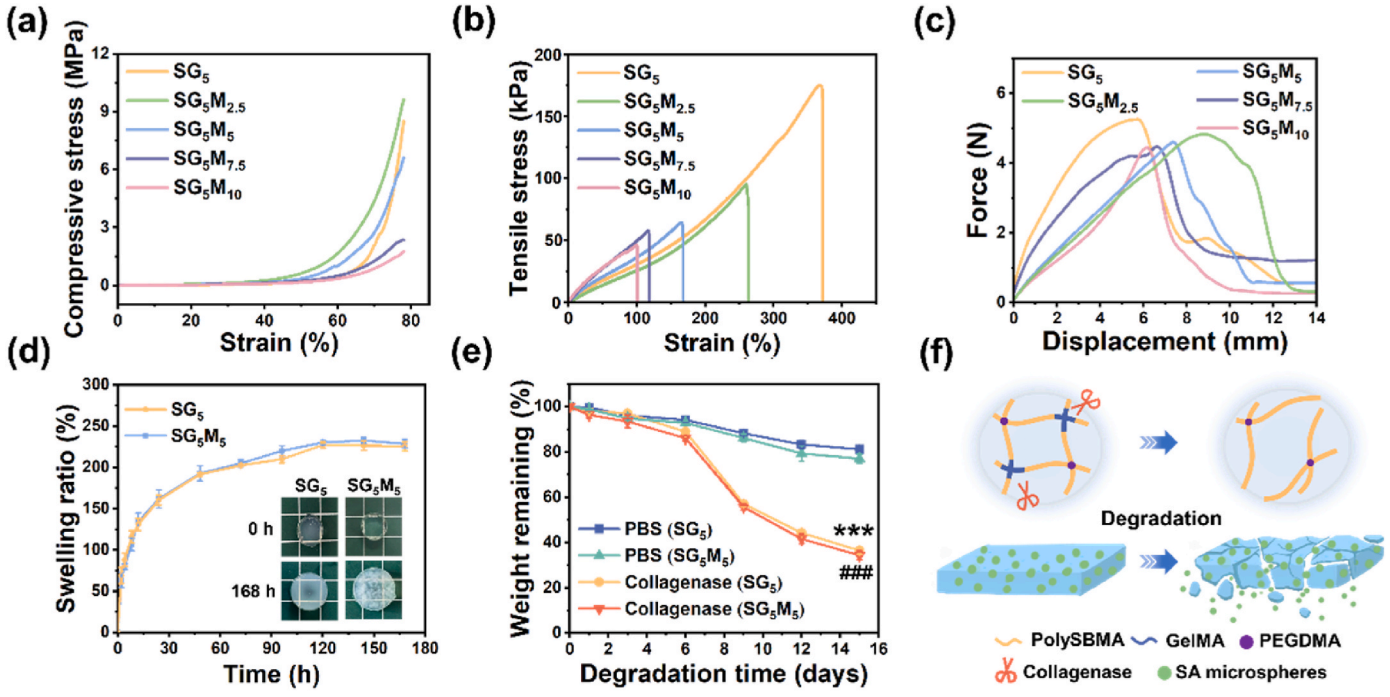

Fig. 5. (a) Representative compressive stress-strain curves, (b) tensile stress-strain curves, and (c) adhesive force-displacement curves (on rabbit fascia) of SG_5 and SG_5M_y hydrogels. (d) Swelling behavior of SG_5 and SG_5M_5 hydrogels. (e) Degradation behavior of SG_5 and SG_5M_5 hydrogels in PBS and collagenase solution (3 U/mL) over 15 days. *** represents significant difference ($p < 0.001$) compared with the PBS (SG_5) group; ### represents significant difference ($p < 0.001$) compared with the PBS (SG_5M_5) group. (f) Schematic illustration of the degradation mechanism of SG_xM_y hydrogel.

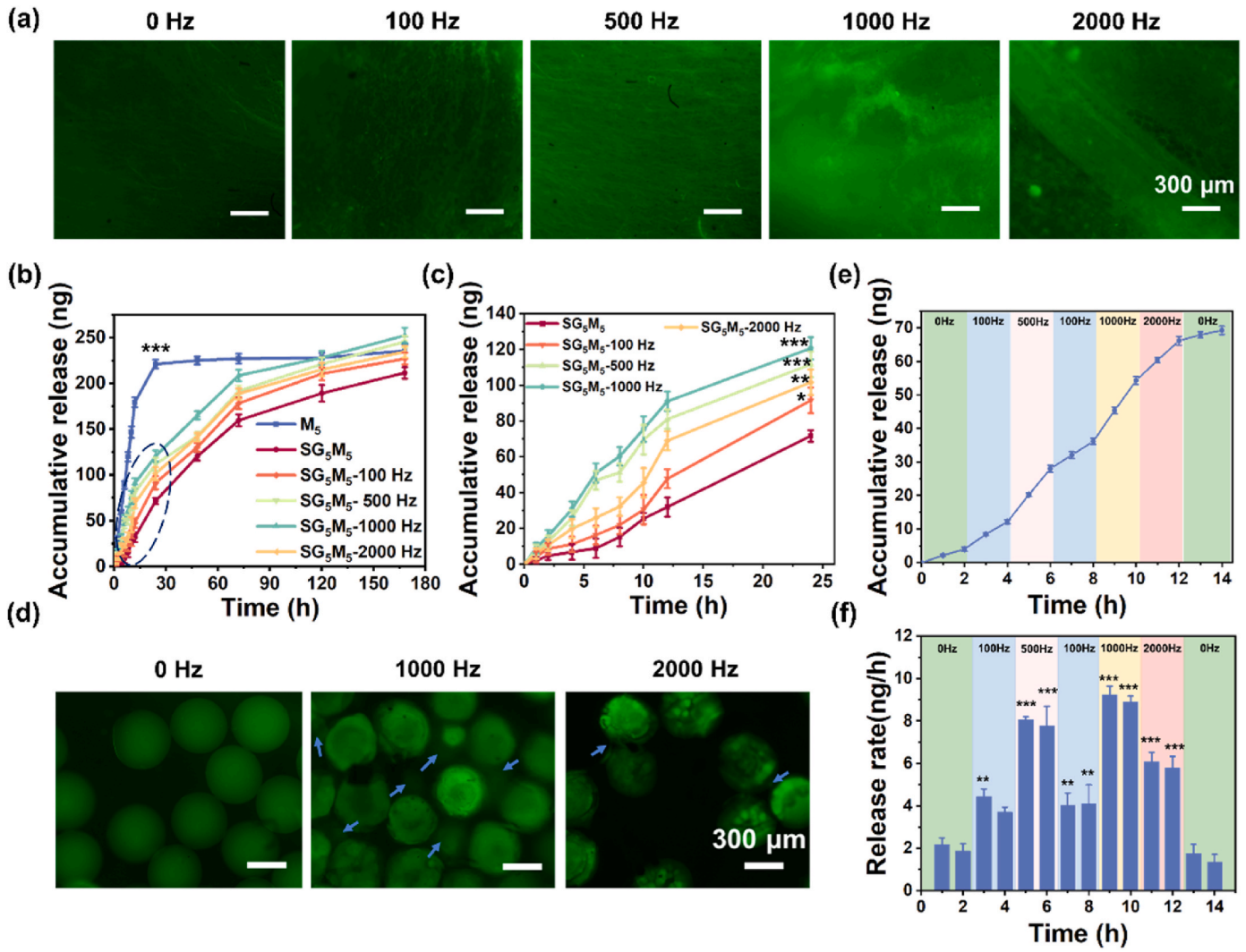

Fig. 6. (a) Representative fluorescent microscope images of bFGF release from SG_5M_5 hydrogel onto rabbit fascia after 2 h of vibration with different vibration frequencies. (b) Drug release from M_5 and SG_5M_5 hydrogel under different vibration conditions in 168 h *** represents significant difference ($p < 0.001$) compared with the SG_5M_5 group. (c) Drug release from SG_5M_5 hydrogel in 24 h *, **, and *** represent significant difference (*$p < 0.05$, **$p < 0.01$, ***$p < 0.001$) compared with the SG_5M_5 group. (d) Representative fluorescent microscope images of SG_5M_5 hydrogels incorporated with FITC-bFGF-loaded SA microspheres after subjecting to vibration at different frequencies for 2 h. Blue arrows indicate bFGF release. (e) Drug release and (f) release rate from SG_5M_5 hydrogel under multi-frequency vibration conditions in 14 h **, and *** represent significant difference (**$p < 0.01$, ***$p < 0.001$) compared with the value at 1 h.

reduce the scattering effect in the hydrogel, resulting in high transmittance [45]. Conversely, a higher GelMA content leads to more intrinsic hydrogen bonding between GelMA chains, resulting in decreased hydrogel transmittance and increased network stability. It is observed that the light transmittance of SG_5 and SG_{10} is lower than that of SG_0 before and after swelling (Fig. 3f).

3.3. Preparation and characterization of microsphere-incorporated hydrogel

To investigate the distribution and stability of the SA microspheres incorporated in the hydrogels containing different GelMA contents, FITC-labeled bFGF was loaded into the SA microspheres and used for the preparation of hydrogels (referred to as SG_xM_y hydrogels). As observed using a fluorescence microscope, the microspheres were uniformly dispersed within the as-prepared SG_xM_5 hydrogels (Fig. 4), and they were deformed after the SG_xM_5 hydrogels being compressed to 80 % and released for 5 cycles, or stretched to 100 %. After compression or stretching, the SG_0M_5 hydrogel exhibited noticeable cracks at the interface between the hydrogel and the microspheres. A portion of the microspheres in the $SG_{2.5}M_5$ hydrogel separated from the hydrogel after being subjected to tensile force. The SG_5M_5 and $SG_{10}M_5$ hydrogels do not exhibit these undesirable cracks or separations when compressed or stretched. This difference could be attributed to the dense network structure of the hydrogels containing high contents of GelMA (5–10 wt %), enabling a strong binding effect of the hydrogel matrix to the SA microspheres. Based on the results above, hydrogels containing 5 wt% of GelMA exhibited superior mechanical properties, adhesion strengths, appropriate swelling capability, and sufficient loading capacity of SA microspheres. Thus, the SG_5 hydrogel was selected for the rest of the study.

The impact of incorporating microspheres on the mechanical and adhesion properties of hydrogels was further investigated. The compressive strength of the hydrogel increased from 8.5 MPa to 9.6 MPa as the concentration of microspheres in the precursor solution increased from 0 wt% to 2.5 wt% (Fig. 5a). However, as the concentration of microspheres increased from 2.5 wt% to 5 wt%, the compressive strength decreased significantly to 6.6 MPa. In addition, when the loading concentration of microspheres exceeded 5 wt%, the hydrogel exhibited diminished resilience and developed cracks when subjected to

compressive forces (Fig. S7). A possible reason for this phenomenon is that a limited number of microspheres can act as robust anchors in hydrogels, thereby enhancing the mechanical strength of the entire system [54]. However, an excessive amount of microspheres can damage the structure of the hydrogel network. Moreover, when the microsphere content increased, the tensile strength significantly declined from 175.2 kPa for SG_5 to 46.7 kPa for SG_5M_{10} (Fig. 5b). In comparison, the adhesive strength of the hydrogels decreased slightly from 52.8 kPa (i.e., 5.28 N) for SG_5 to 45.1 kPa (i.e., 4.51 N) for SG_5M_{10} (Fig. 5c). Based on the evaluation of the compressive, tensile, and adhesion properties, as well as the growth factor loadings of hydrogels, microspheres at a concentration of 5 wt% were considered suitable for the preparation of hydrogels. The SG_5M_5 hydrogel exhibited satisfactory mechanical properties and adhesion performance, which are beneficial for healing perforated TMs. The compressive strength, tensile strength, and adhesion strength of SG_5M_5 hydrogel were 6.6 MPa, 64.1 kPa, and 45.6 kPa (i.e., 4.56 N), respectively. The mechanical properties of SG_5M_5 hydrogels are higher than adipose tissue [55]and GelMA-keratin methacryloyl hydrogels [52] reported in the literature, and it is expected that they are adequate for TM perforation repair.

As shown in Fig. 5d, the presence of microspheres did not significantly impact the swelling performance of the hydrogel. The hydrogel remained stable after reaching swelling equilibrium and did not show any apparent decomposition. Treatment of TM perforation with growth factors typically takes about two weeks [56]. The hydrogel remained relatively stable in PBS, with over 72 % of its mass remaining in both static conditions (Fig. 5e) and vibration conditions after 15 days (Fig. S8). This allows it to provide continuous support throughout the healing process without degrading or being absorbed too quickly. Additionally, collagenase can break down the hydrogel by degrading the GelMA cross-linking sites (Fig. 5f) [57], allowing the hydrogel to degrade and be removed after the perforation is healed. Under vibration conditions, the vibration mechanical force will accelerate the degradation of hydrogel and the mass of the hydrogel is about 20–30 % after 15 days (Fig. S8b). Importantly, this degradation is unlikely to cause a foreign body reaction on the TM that could interfere with sound conduction.

3.4. Mechano-responsive release of bFGF from hydrogels

Stimuli-responsive hydrogels are gaining popularity in drug delivery due to their intelligent design [58]. The application of mechano-responsive hydrogels is considered an advanced and promising strategy for controlling drug delivery in dynamic wound environments. This is due to the readily available and easily controlled nature of mechanical stimuli compared to traditional chemical and biological stimuli. TM perforation is a prevalent condition in otolaryngology, and drug-carrying hydrogels offer a novel option for the clinical treatment of TM. It is widely recognized that acoustic waves cause vibrations of the TM. However, traditional drug delivery systems only consider passive drug delivery in static environments. Inactive drug delivery is uncontrollable in terms of the amount of drug released, which fails to meet the varying drug demands during different stages of TM repair and does not promote the healing of the perforation. Considering the dynamic mechanical environment at the site of a TM perforation, clinical control of drug release can be achieved by using earplugs to block sound waves or providing auditory stimuli at different frequencies. Therefore, developing a hydrogel with mechano-responsive drug release would provide a novel and effective approach to treating TM perforation in clinical practice. In this study, the release properties of bFGF from SG_5M_5 hydrogels were investigated, with a specific focus on their response to various vibration and sound stimulation conditions.

As shown in Fig. 6a, the fluorescence intensity on the rabbit fascia exhibited a gradual increase with an increase in vibration frequency from 0 Hz to 1000 Hz. Conversely, a gradual decrease in fluorescence intensity was observed with an increase in vibration frequency from 1000 Hz to 2000 Hz. These initial findings indicated that within the frequency range of 0–2000 Hz, the release of bFGF tended to respond mechanically to the vibration frequency. Subsequently, the release of bFGF over prolonged periods was quantified using the ELISA kit. The results in Fig. 6b demonstrate that SA microspheres alone induced a burst release of bFGF, reaching the maximum release within approximately 24 h. However, the therapeutic effect of bFGF was primarily manifested after 3–4 days following TM perforation [10]. Incorporating bFGF-loaded microspheres in a hydrogel matrix facilitated the sustained release of the growth factor. The duration of bFGF release from SG_5M_5 hydrogel without vibration extended beyond one week, effectively meeting the requirement for promoting TM perforation. The results indicate that the cumulative release of bFGF from the hydrogel increased as the vibration frequency increased to 1000 Hz (Fig. 6b and c). The release of bFGF significantly increased after one day of exposure to a vibration frequency of 1000 Hz compared to the condition without vibration. The cumulative release contents increased from 71.7 $\pm$ 3.2 ng to 120.7 $\pm$ 6.2 ng (Fig. 6c). This phenomenon may be attributed to the hydrogel deforming and the network structure becoming loose under the influence of the vibration force, leading to the deformation of the microspheres and the release of the drugs. As shown in Fig. 6d, under the influence of the vibration force, the morphology of the microspheres changes, leading to an uneven internal fluorescence distribution. The fluorescent bFGF that accumulated at the periphery of the microspheres was subsequently released into the hydrogel matrix and finally diffused into the surrounding aqueous environment, as indicated by the blue arrows. This mechanism makes it possible to control drug release from the hydrogel through vibration stimulation. The mechanism is more intuitive in the presence of tensile forces, as illustrated in Fig. S9a, which depicts the deformation of microspheres under tensile forces applied to the hydrogel and their subsequent return to their original shape upon the withdrawal of the forces. Drug release can be observed in the vicinity of the microspheres following ten cycles of stretching. A statistical analysis of the length-to-diameter ratio of microspheres revealed that the ratio of undergoing stretching microspheres exhibited a markedly higher value than that observed prior to stretching (Fig. S9b). However, no statistically significant difference was identified in the length-to-diameter ratio of the microspheres prior to and following stretching. It supports the conclusion that microspheres are capable of reversible deformation under the influence of mechanical force. The results above indicate the mechano-responsiveness of microsphere-incorporated hydrogel. However, when the vibration frequency increased from 1000 Hz to 2000 Hz, the cumulative release of bFGF from the hydrogel over 24 h decreased to 101.7 $\pm$ 7.2 ng. This decrease may be attributed to the relatively low amplitude of vibration at a high frequency. Since the TM is exposed to sound stimulation in daily life, the hydrogel was placed on top of a playing radio to simulate the drug release behavior under the influence of sound stimulus. The release of bFGF was significantly increased after one day of sound stimulation compared to the control group. The cumulative release contents over 24 h increased from 74.6 $\pm$ 4.6 ng to 100.4 $\pm$ 4.0 ng (Fig. S10). The results confirm that the hydrogels are capable of releasing bFGF in response to sound stimulation, which is suitable for the physiological environment of the TM.

Furthermore, the mechano-responsive release of the hydrogel under multi-frequency vibration conditions was investigated (Fig. 6e and f). The release rate of bFGF exhibits a notable variation in response to alterations in vibration frequency over 14 h. Specifically, the release rate can be enhanced from 1.4 $\pm$ 0.4 ng/h at 0 Hz to 9.3 $\pm$ 0.4 ng/h at 1000 Hz, while it can be diminished to 5.8 $\pm$ 0.5 ng/h at a frequency of 2000 Hz, probably due to the relatively low amplitude at 2000 Hz. The findings further confirm that the hydrogels are capable of releasing bFGF in response to vibration stimuli.

Additionally, it was observed from Fig. S11 that the increase in vibration frequency did not significantly impact the compression strength of the hydrogel, thereby demonstrating that the mechanical properties

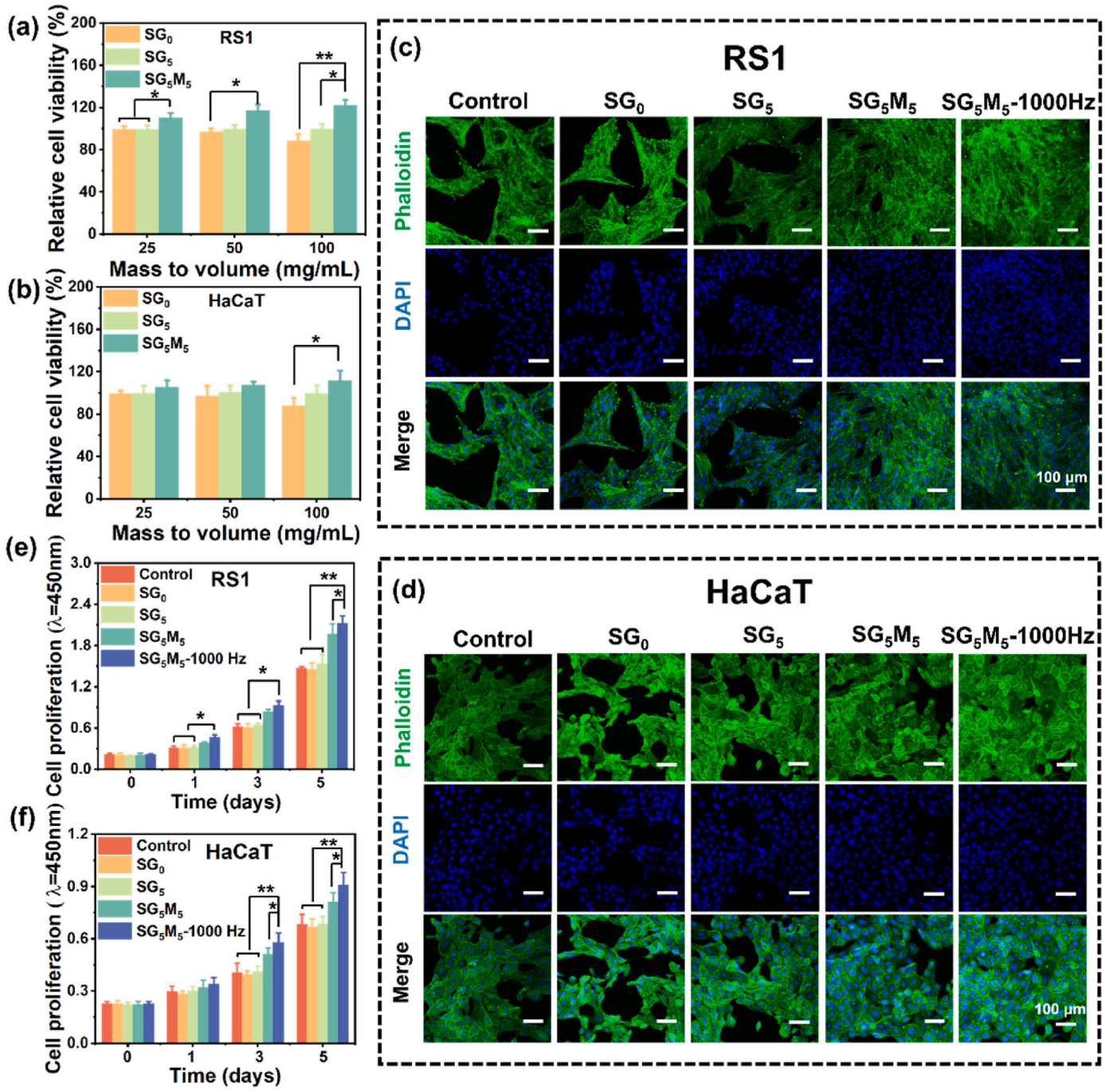

Fig. 7. Relative cell viability of (a) RS1 cells and (b) HaCaT cells after incubation in hydrogel extract with various dilution ratios for 24 h. Fluorescent images of (c) RS1 cells and (d) HaCaT cells cultured in hydrogel extracts (50 mg hydrogel per mL) for 5 days and stained by phalloidin and DAPI. Cell proliferation of (e) RS1 cells and (f) HaCaT cells after being cultured in hydrogel extracts (50 mg hydrogel per mL) for 5 days was quantified using the CCK-8 assay.

of the hydrogel remained unaffected by vibrations. These findings provide evidence supporting the potential use of the SG_5M_5 hydrogel as a promising material for repairing TM perforations under mechanical vibration conditions.

3.5. Biocompatibility and cell proliferation

The biomaterials used in tympanic tissue engineering must have non-toxic, non-allergenic, and biocompatible properties to ensure their biosafety during perforation treatment. The healing process of a perforated TM typically involves three stages [59,60]. Firstly, an inflammatory reaction occurs, causing the squamous epithelium at the edge of the perforation to become hyperplastic and exhibit excessive keratin production. Secondly, the perforation is closed through the proliferation and migration of the squamous epithelium. Finally, the three-layer structure of the TM is restored through fibroblast activity, vasculogenesis, and angiogenesis. The biocompatibility and bioactivity of the hydrogels were assessed using epithelial cells (HaCaT cells) and fibroblasts (RS1 cells). Firstly, potential cytotoxicity was evaluated by culturing the cells with hydrogel extracts. The viability of cells in all groups (i.e., SG_0, SG_5, and SG_5M_5 hydrogels with different extraction conditions) remained high after incubation for 24 h (Fig. 7a and b), with a relative viability rate exceeding 80 %. All types of hydrogels exhibited minimal cytotoxicity, indicating their excellent cytocompatibility.

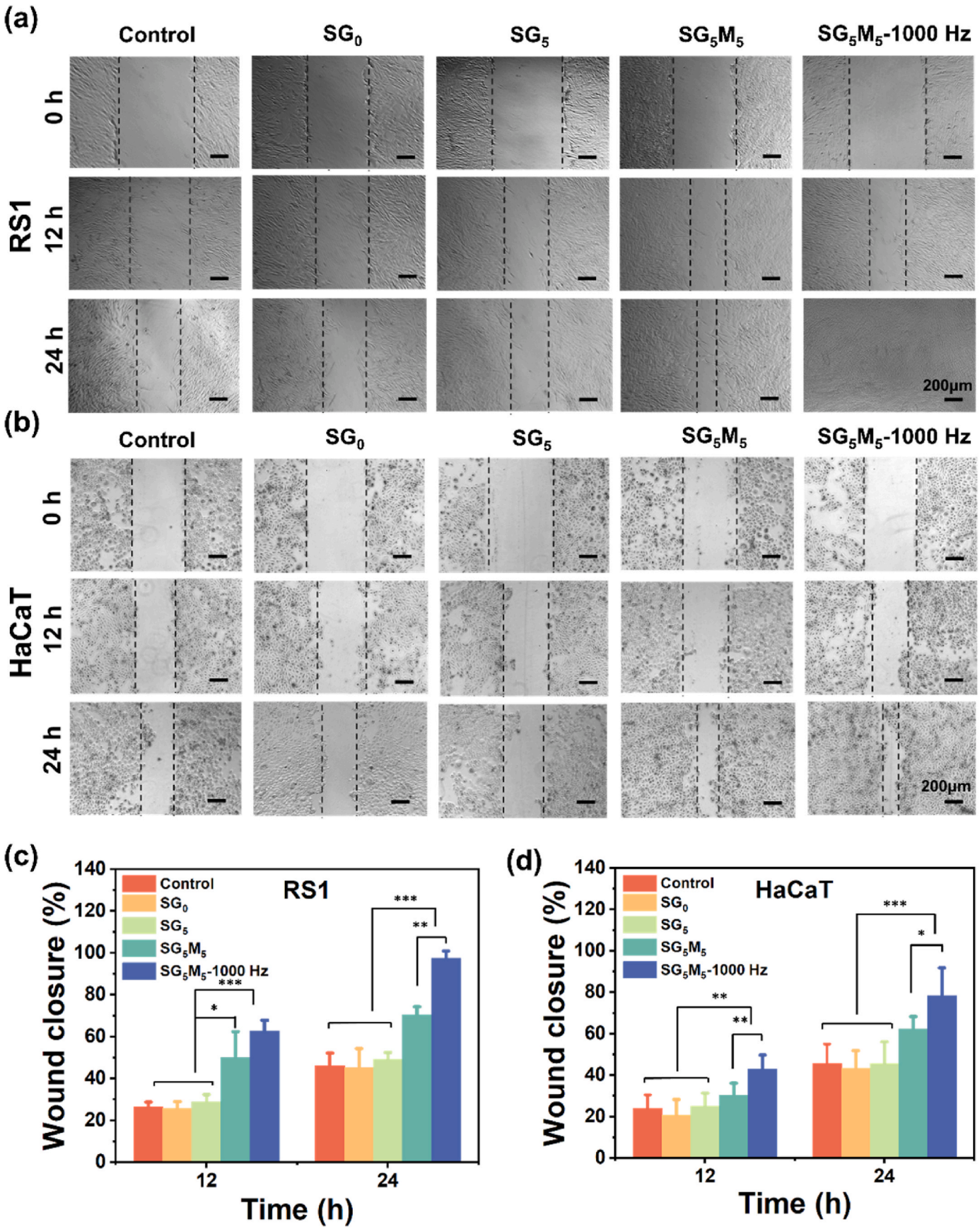

Fig. 8. Digital microscopy images of the migration of (a) RS1 cells and (b) HaCaT cells after being cultured in hydrogel extracts (50 mg hydrogel per mL) for 24 h. The quantitative analysis of the migration of (c) RS1 cells and (d) HaCaT cells after being cultured in hydrogel extracts (50 mg hydrogel per mL) for 12 and 24 h.

The role of bFGF in the proliferative phase of TM perforation (3–4 days after injury) is crucial [10], as it promotes the proliferation of epithelial cells, especially fibrocytes [61,62]. The biological activity of extracts incubated with SG_5, SG_0, and SG_5M_5 hydrogels statically, and with SG_5M_5 hydrogel vibrated at 1000 Hz after 1, 3, and 5 days was assessed using a cell proliferation assay (Fig. 7c and d, S12, and S13). These images display the shapes of cells in two dimensions using F-actin labeling (green fluorescence with phalloidin). All cell groups exhibit vigorous growth with well-defined nuclei (blue fluorescence with DAPI). The RS1 cells were spindle-shaped, while the HaCaT cells were irregularly polygonal. Furthermore, cells extend into adjacent cells, forming a reticular cytoskeletal network. This phenomenon is particularly noticeable in RS1 cells. It is worth noting that the SG_5M_5-1000 Hz group had the highest cell count and displayed superior cell morphology. The experimental results indicate that the hydrogel released bFGF, which stimulated the growth of epithelial cells and fibroblasts. Furthermore, the hydrogel released more bFGF when subjected to vibration, which enhanced cell proliferation. Live/dead cell staining images showed a similar cell growth pattern to the immunofluorescence staining results (Fig. S14). Given that the regeneration of blood vessels also plays a role in the healing of TM perforation, we included the HUVEC cell group in the experiments (Fig. S14), which showed that HUVEC cells exhibited a similar growth pattern as the RS1 and HaCaT cells, indicating that bFGF released from hydrogel can stimulate the growth of vascular endothelial cells.

The quantification results showed that the SG_0 group had the lowest cell proliferation rate (Fig. 7e and f). There was no statistical difference in the value-added rate between the SG_5 and control groups over a 5-day culture period. In contrast, the proliferation rate of the cells in the SG_5M_5 and SG_5M_5-1000 Hz groups was significantly higher than that of the control group. Notably, the proliferation rate of the SG_5M_5-vibration group was the highest. The findings suggest that the SG_5M_5 and SG_5M_5-1000 Hz groups, loaded with bFGF, could potentially promote the growth and proliferation of RS1 cells and HaCaT cells. In contrast, the SG_0 and SG_5 groups contained no bFGF and had no significant effect on cell proliferation. The above results demonstrate that the released active bFGF, but not the hydrogel alone, showed a promotive effect on cell proliferation. Under the influence of vibrational force, more bFGF can be released from the hydrogel to meet the needs for the dynamic repair of TM perforation under physiological conditions.

SG_5M_5 hydrogel would be applied as an adhesive material to a damaged TM. As SG_5M_5 hydrogel degrades, it will be replaced by natural tissue as a result of cell migration and growth on the surface and in the hydrogel, which consequently results in the formation of new tissue at the damaged site. To simulate the above processes, RS1 cells were embedded within the hydrogel, and HaCaT cells were cultured on the hydrogel surface. As shown in Fig. S15, a notable elevation in the number of HaCaT cells on the surface of the hydrogel, as well as RS1 cells inside the hydrogel, was discerned over five days of incubation. The results demonstrated that SG_5M_5 hydrogel is a favorable material for cell growth and potentially promising for TM tissue engineering.

3.6. Cell migration

The presence of bFGF induces the migration of keratinocytes at the perforation boundary and exerts a significant pro-migratory effect on cells within the intermediate fibrous layer [10]. Thus, a cell migration assay was performed to assess the quantity and activity of the released bFGF from hydrogels. In addition, the cell migration assay can simulate an *in vitro* wound healing experiment and evaluate the potential of hydrogels to promote wound healing by enhancing cell migration. After 24 h of culturing, the scratches were visibly closed by migrated RS1 cells and HaCaT cells in the SG_5M_5 and SG_5M_5-1000 Hz groups (Fig. 8a and b), while fewer migrated cells were observed in the SG_0, SG_5, and control groups. The quantitative results demonstrate that both the SG_5M_5 and SG_5M_5-1000 Hz groups show the ability to enhance the migration speed of RS1 cells and HaCaT cells under the influence of growth factors, with the SG_5M_5-1000 Hz group hydrogel displaying the highest rate of cell migration (Fig. 8c and d). These findings suggest that the hydrogel has bioactive bFGF release capabilities, and vibration can further enhance the release rate to promote cell migration. The concurrent evidence also indicates the potential of bFGF-loaded hydrogel in promoting wound healing.

To further investigate the migrating capacity of cells on hydrogels, RS1 and HaCaT cells were seeded on one half of the surface of a SG_5M_5 hydrogel disk, and then the cells were cultured to allow them to migrate to the surface of the other half of the hydrogel (Fig. S16a). As shown in Fig. S16b, cell growth was observed in and around the incised edges of the second half of the hydrogel, demonstrating that cells can migrate on the hydrogel surface. It is therefore anticipated that this biomaterial permits cell migration for effectively repairing TM perforations.

4. Conclusions

In summary, the present study has successfully developed a mechano-responsive hydrogel for the controlled release of bFGF, demonstrating excellent mechanical properties and tissue adhesion capabilities. When mechanical force is applied, the network structure of the hydrogel undergoes relaxation, leading to the deformation of drug-loaded microspheres and, consequently, enhancing drug release. Thus, the mechano-responsive drug release profile from the hydrogel can be obtained. This hydrogel also demonstrates excellent biocompatibility with mammalian cells. The active growth factors released by the hydrogel effectively stimulate cell proliferation and migration. The tough, mechano-responsive hydrogel capable of releasing bFGF shows great potential as a scaffold for promoting the healing of TM perforations in a vibrational environment.

CRediT authorship contribution statement

Shengjia Chen: Writing – original draft, Validation, Resources, Methodology, Investigation, Formal analysis, Data curation, Conceptualization. **Xiangshu Guo:** Validation, Data curation. **Yanyu Yang:** Data curation. **Junjie Deng:** Visualization. **Ting Xu:** Methodology. **Zhechen Yuan:** Methodology. **Hao Xue:** Investigation. **Longxing Niu:** Writing – review & editing, Validation, Investigation, Formal analysis. **Rong Wang:** Writing – review & editing, Supervision, Project administration, Funding acquisition, Formal analysis, Conceptualization. **Yi Shen:** Writing – review & editing, Supervision, Funding acquisition, Conceptualization.

Declaration of competing interest

The authors declare that they have no known competing financial interests or personal relationships that could have appeared to influence the work reported in this paper.

Data availability

Data will be made available on request.

Acknowledgements

This study was supported by Natural Science Foundation of Zhejiang Province (LY23H130001), Zhejiang Provincial Medical and Health Science Research Foundation (2020KY274 and 2022KY1086), National Natural Science Foundation of China (81670920), Ningbo Public Science Research Foundation (2021S170), Natural Science Foundation of Ningbo (2022J260), Youth Innovation Promotion Association CAS (2021296), Key Research and Development Program of Ningbo (2022Z132), and Foundation of Director of Ningbo Institute of Materials Technology and Engineering CAS (2021SZKY0301).

Appendix A. Supplementary data

Supplementary data to this article can be found online at https://doi.org/10.1016/j.mtbio.2024.101212.

References

[1] X. Yao, B.M. Teh, H. Li, Y. Hu, J. Huang, C. Lv, S. Bu, M. Zheng, Y. Shen, Acellular collagen scaffold with basic fibroblast growth factor for repair of traumatic tympanic membrane perforation in a rat model, Otolaryngol. Head Neck Surg. 164 (2) (2021) 381–390.

[2] Z. Hussain, R. Pei, Necessities, opportunities, and challenges for tympanic membrane perforation scaffolding-based bioengineering, Biomed. Mater. 16 (3) (2021) 032004.

[3] J. Huang, B.M. Teh, R.H. Eikelboom, L. Han, G. Xu, X. Yao, Y. Hu, M. Zheng, Y. Shen, The effectiveness of bFGF in the treatment of tympanic membrane perforations: a systematic review and meta-analysis, Otol. Neurotol. 41 (6) (2020) 782–790.

[4] C.H. Jang, W. Kim, C. Moon, G. Kim, Bioprinted collagen-based cell-laden scaffold with growth factors for tympanic membrane regeneration in chronic perforation model, IEEE Trans. Nanobiosci 21 (3) (2022) 370–379.

[5] E. Ilhan, S. Ulag, A. Sahin, B.K. Yilmaz, N. Ekren, O. Kilic, M. Sengor, D. M. Kalaskar, F.N. Oktar, O. Gunduz, Fabrication of tissue-engineered tympanic membrane patches using 3D-printing technology, J. Mech. Behav. Biomed. Mater. 114 (2021) 104219–104230.

[6] S. Mahdiani, L. Lasminingrum, D. Anugrah, Management evaluation of patients with chronic suppurative otitis media: a retrospective study, Ann. Med. Surg. 67 (2021) 102492–102496.

[7] J. Huang, Y. Shi, L. Wu, C. Lv, Y. Hu, Y. Shen, Comparative efficacy of platelet-rich plasma applied in myringoplasty: a systematic review and Meta-analysis, PLoS One 16 (1) (2021) e0245968.

[8] Z. Lou, Z. Lou, Z. Chen, Effect of packing versus no packing in transperforation myringoplasty for chronic tympanic membrane perforations, Otolaryngol. Head Neck Surg. 169 (5) (2023) 1170–1178.

[9] Z.C. Lou, Z.H. Lou, J. Xiao, Regeneration of the tympanic membrane using fibroblast growth factor-2, J. Laryngol. Otol. 132 (6) (2018) 470–478.

[10] M. Jeong, K. Bojkovic, V. Sagi, K.M. Stankovic, Molecular and clinical significance of fibroblast growth factor 2 in development and regeneration of the auditory system, Front. Mol. Neurosci. 14 (2021) 757441–757458.

[11] F. Santos, E. Shu, D.J. Lee, D.H. Jung, A.M. Quesnel, K.M. Stankovic, D.E. Abdul-Aziz, C.P. Bay, A. Quinkert, D.B. Welling, A. Quinkert, D.B. Welling, Topical fibroblast growth factor-2 for treatment of chronic tympanic membrane perforations, Laryngoscope Investig Otolaryngol 5 (4) (2020) 657–664.

[12] N. Azarpira, M. Kaviani, F.S. Sarvestani, Incorporation of VEGF-and bFGF-loaded alginate oxide particles in acellular collagen-alginate composite hydrogel to promote angiogenesis, Tissue Cell 72 (2021) 101539–101545.

[13] G.W. Cho, C. Moon, A. Song, K.A. Vijayakumar, M.J. Ang, C.H. Jang, Effect of growth factor-loaded acellular dermal Matrix/MSCs on regeneration of chronic tympanic membrane perforations in rats, J. Clin. Med. 10 (7) (2021) 1541–1556.

[14] Z.C. Lou, Z.H. Lou, A moist edge environment aids the regeneration of traumatic tympanic membrane perforations, J. Laryngol. Otol. 131 (7) (2017) 564–571.

[15] Y. Wang, F. Wen, X. Yao, L. Zeng, J. Wu, Q. He, H. Li, L. Fang, Hybrid hydrogel composed of hyaluronic acid, gelatin, and extracellular cartilage matrix for perforated TM repair, Front. Bioeng. Biotechnol. 9 (2021) 811652–811671.

[16] B. Wang, T. Xin, L. Shen, K. Zhang, D. Zhang, H. Zhang, J. Liu, B. Chen, W. Cui, Y. Shu, Acoustic transmitted electrospun fibrous membranes for tympanic membrane regeneration, Chem. Eng. J. 419 (2021) 129536, 123552.

[17] P.L. Santa Maria, S. Kim, Y.K. Varsak, Y.P. Yang, Heparin binding-epidermal growth factor-like growth factor for the regeneration of chronic tympanic membrane perforations in mice, Tissue Eng. Part A 21 (9–10) (2015) 1483–1494.

[18] X. Khoo, E.J. Simons, H.H. Chiang, J.M. Hickey, V. Sabharwal, S.I. Pelton, J. J. Rosowski, R. Langer, D.S. Kohane, Formulations for trans-tympanic antibiotic delivery, Biomaterials 34 (4) (2013) 1281–1288.

[19] K. Fang, R. Wang, H. Zhang, L. Zhou, T. Xu, Y. Xiao, Y. Zhou, G. Gao, J. Chen, D. Liu, F. Ai, J. Fu, Mechano-responsive, tough, and antibacterial zwitterionic hydrogels with controllable drug release for wound healing applications, ACS Appl. Mater. Interfaces 12 (47) (2020) 52307–52318.

[20] J. Di, S. Yao, Y. Ye, Z. Cui, J. Yu, T.K. Ghosh, Z. Gu, Stretch-triggered drug delivery from wearable elastomer films containing therapeutic depots, ACS Nano 9 (9) (2015) 9407–9415.

[21] L.M. Caballero Aguilar, S. Duchi, C. Onofrillo, C.D. O'Connell, C. Di Bella, S. E. Moulton, Formation of alginate microspheres prepared by optimized microfluidics parameters for high encapsulation of bioactive molecules, J. Colloid Interface Sci. 587 (2021) 240–251.

[22] S. Utech, R. Prodanovic, A.S. Mao, R. Ostafe, D.J. Mooney, D.A. Weitz, Microfluidic generation of monodisperse, structurally homogeneous alginate microgels for cell encapsulation and 3D cell culture, Adv. Healthcare Mater. 4 (11) (2015) 1628–1633.

[23] M. Keykhaee, M. Rahimifard, A. Najafi, M. Baeeri, M. Abdollahi, F. Mottaghitalab, M. Farokhi, M. Khoobi, Alginate/gum Arabic-based biomimetic hydrogel enriched with immobilized nerve growth factor and carnosine improves diabetic wound regeneration, Carbohydr. Polym. 321 (2023) 121179–121199.

[24] S. Mohammadi, S. Ramakrishna, S. Laurent, M.A. Shokrgozar, D. Semnani, D. Sadeghi, A. Res, S. Bonakdar, M. Akbari, Fabrication of nanofibrous PVA/alginate-sulfate substrates for growth factor delivery, J. Biomed. Mater. 107 (2) (2018) 403–413.

[25] R. Zhang, L. Xie, H. Wu, T. Yang, Q. Zhang, Y. Tian, Y. Liu, X. Han, W. Guo, M. He, S. Liu, W. Tian, Alginate/laponite hydrogel microspheres co-encapsulating dental pulp stem cells and VEGF for endodontic regeneration, Acta Biomater. 113 (2020) 305–316.

[26] J.S. Farrelly, A.H. Bianchi, A.S. Ricciardi, G.L. Buzzelli, S.L. Ahle, M.R. Freedman-Weiss, D.H. Stitelman, Alginate microparticles loaded with basic fibroblast growth factor induce tissue coverage in a rat model ofmyelomeningocele, J. Pediatr. Surg. 54 (1) (2019) 80–85.

[27] O. Zuo, R. Guo, Q. Liu, A. Hong, Y. Shi, Q. Kong, W. Xue, Heparin-conjugated alginate multilayered microspheres for controlled release of bFGF, Biomed.Mater. 10 (3) (2015) 035008.

[28] Q. Liu, Y. Huang, Y. Lan, Q. Zuo, C. Li, Y. Zhang, W. Xue, Acceleration of skin regeneration in full-thickness burns by incorporation of bFGF-loaded alginate microspheres into a CMCS–PVA hydrogel, J. Tissue Eng Regen. M. 11 (5) (2017) 1562–1573.

[29] Z. Xiao, X. Zheng, Y. An, K. Wang, J. Zhang, H. He, J. Wu, Zwitterionic hydrogel for sustained release of growth factors to enhance wound healing, Biomater. Sci. 9 (3) (2021) 882–891.

[30] Y. Zhu, J. Zhang, J. Yang, C. Pan, T. Xu, L. Zhang, Zwitterionic hydrogels promote skin wound healing, J. Mater. Chem. B 4 (30) (2016) 5105–5111.

[31] H. He, Z. Xiao, Y. Zhou, A. Chen, X. Xuan, Y. Li, X. Guo, J. Zheng, J. Xiao, J. Wu, Zwitterionic poly (sulfobetaine methacrylate) hydrogels with optimal mechanical properties for improving wound healing *in vivo*, J. Mater. Chem. B 7 (10) (2019) 1697–1707.

[32] G. Lan, S. Zhu, D. Chen, H. Zhang, L. Zou, Y. Zeng, Highly adhesive antibacterial bioactive composite hydrogels with controllable flexibility and swelling as wound dressing for full-thickness skin healing, Front. Bioeng. Biotechnol. 9 (2021) 785302–785314.

[33] A.G. Kurian, R.K. Singh, K.D. Patel, J.H. Lee, H.W. Kim, Multifunctional GelMA platforms with nanomaterials for advanced tissue therapeutics, Bioact. Mater. 8 (2022) 267–295.

[34] K. Yue, G.T. Santiago, M.M. Alvarez, A. Tamayol, N. Annabi, A. Khademhosseini, Synthesis, properties, and biomedical applications of gelatin methacryloyl (GelMA) hydrogels, Biomaterials 73 (2015) 254–271.

[35] Y. Liu, T. Li, M. Sun, Z. Cheng, W. Jia, K. Jiao, S. Wang, K. Jiang, Y. Yang, Z. Dai, L. Liu, G. Liu, Y. Luo, ZIF-8 modified multifunctional injectable photopolymerizable GelMA hydrogel for the treatment of periodontitis, Acta Biomater. 146 (2022) 37–48.

[36] G.F. Karianne, H. Astrid, E. Caroline, B. Sopisa, L.S. Berit, L.D. Catharina, M. Ýrr, K. Flatmark, Alginate microsphere encapsulation of drug-loaded nanoparticles: a novel strategy for intraperitoneal drug delivery, Mar. Drugs 20 (12) (2022) 744–757.

[37] Q. Zuo, J. Lu, A. Hong, D. Zhong, S. Xie, Q. Liu, Y. Huang, Y. Shi, L. He, W. Xue, Preparation and characterization of PEM-coated alginate microgels for controlled release of protein, Biomed. Mater. 7 (3) (2012) 035012.

[38] P. Izharuddin, J. Gupta, K.V.R. Reddy, Alginate microspheres: the innovative approaches to production of the microbeads/micro-particles, J. Drug Deliv. Ther. 9 (4-s) (2019) 774–781.

[39] A. Partovinia, E. Vatankhah, Experimental investigation into size and sphericity of alginate micro-beads produced by electrospraying technique: operational condition optimization, Carbohydr. Polym. 209 (2019) 389–399.

[40] B.B. Lee, P. Ravindra, E.S. Chan, Size and shape of calcium alginate beads produced by extrusion dripping, Chem. Eng. Technol. 36 (10) (2013) 1627–1642.

[41] G. Ciarleglio, T. Russo, E. Toto, M.G. Santonicola, Fabrication of alginate/ozoile gel microspheres by electrospray process, Gels 10 (1) (2024) 52–67.

[42] M. Alfatama, Y. Shahzad, H. Choukaife, Recent advances of electrospray technique for multiparticulate preparation: drug delivery applications, Adv. Colloid Interface Sci. 325 (2024) 103098–103115.

[43] Y. Fang, S. Huang, X. Gong, J.A. King, Y. Wang, J. Zhang, X. Yang, Q. Wang, Y. Zhang, G. Zhai, L. Ye, Salt sensitive purely zwitterionic physical hydrogel for prevention of postoperative tissue adhesion, Acta Biomater. 158 (2023) 239–251.

[44] R. Kadri, K. Elkhoury, G. Ben Messaoud, C. Kahn, A. Tamayol, J.F. Mano, E. Arab-Tehrany, L. Sánchez-González, Physicochemical interactions in nanofunctionalized alginate/GelMA IPN hydrogels, Nanomaterials 11 (9) (2021) 2256–2265.

[45] M. He, L. Chen, L. Zhang, L. Shen, H. Zhen, L. Wang, P. Xu, J. Bao, A Zwitterion-based hydrogel with high-strength, high transparency, anti-adhesion and degradability, J. Mater. Sci. 57 (35) (2022) 16830–16841.

[46] M. Aleemardani, Z. Bagher, M. Farhadi, H. Chahsetareh, R. Najafi, B. Eftekhari, A. Seifalian, Can tissue engineering bring hope to the development of human tympanic membrane? Tissue Eng., Part B 27 (6) (2021) 572–589.

[47] L. Wang, G. Gao, Y. Zhou, T. Xu, J. Chen, R. Wang, R. Zhang, J. Fu, Tough, adhesive, self-healable, and transparent ionically conductive zwitterionic nanocomposite hydrogels as skin strain sensors, ACS Appl. Mater. Interfaces 11 (3) (2018) 3506–3515.

[48] C.K. Roy, H.L. Guo, T.L. Sun, A.B. Ihsan, T. Kurokawa, M. Takahata, T. Nonoyama, T. Nakajima, J.P. Gong, Self-adjustable adhesion of polyampholyte hydrogels, Adv. Mater. 27 (45) (2015) 7344–7348.

[49] H. Chahsetareh, F. Yazdian, M. Pezeshki-Modaress, M. Aleemardani, S. Hassanzadeh, R. Najafi, S. Simorgh, V. Taghdiri Nooshabadi, Z. Bagher, S. M. Davachi, Alginate hydrogel-PCL/gelatin nanofibers composite scaffold containing mesenchymal stem cells-derived exosomes sustain release for regeneration of tympanic membrane perforation, Int. J. Biol. Macromol. 262 (2024) 130141–130155.

[50] A. Wani, A. Rehman, S. Lateef, R. Malik, A. Ahmed, W. Ahmad, M. Kirmani, Traumatic tympanic membrane perforation: an overview, Indian J. Otol. 22 (2) (2016) 100–104.
[51] S.A. Olowookere, T.S. Ibekwe, A.A. Adeosun, Patterns of tympanic membrane perforation in Ibadan: a retrospective study, Ann. Ib. Postgrad. M. 6 (2) (2008) 31–33.
[52] T. Bedir, D. Baykara, R. Yildirim, A.C. Calikoglu Koyuncu, A. Sahin, E. Kaya, G. B. Tinaz, M.A. Insel, M. Topuzogulları, O. Gunduz, C.B. Ustundag, R. Narayan, Three-dimensional-printed GelMA-KerMA composite patches as an innovative platform for potential tissue engineering of tympanic membrane perforations, Nanomaterials 14 (7) (2024) 563–588.
[53] Z. Zhang, Q. Dou, S. Wang, D. Hu, B. Yang, Z. Zhao, H. Liu, Q. Dai, The development of an antifouling interpenetrating polymer network hydrogel film for salivary glucose monitoring, Nanoscale 12 (44) (2020) 22787–22797.
[54] S. Zhang, A. Lin, Z. Tao, Y. Fu, L. Xiao, G. Ruan, Y. Li, Microsphere-containing hydrogel scaffolds for tissue engineering, Chem. Asian J. 17 (20) (2022) e202200630.
[55] N. Alkhouli, J. Mansfield, E. Green, J. Bell, B. Knight, N. Liversedge, J.C. Tham, R. Welbourn, A.C. Shore, K. Kos, C.P. Winlove, The mechanical properties of human adipose tissues and their relationships to the structure and composition of the extracellular matrix, Am. J. Physiol.-Endoc. M. 305 (12) (2013) 1427–1435.
[56] S. Xu, J. Yu, Y. Hu, B. Yang, N. Yang, The effectiveness and safety of growth factors in the treatment of tympanic membrane perforations: a systematic review and Meta-analysis of randomized controlled trials, Eur. Arch. Oto-Rhino-Laryngol. 279 (4) (2021) 1863–1874.
[57] J. Liang, Z. Wang, A.A. Poot, D.W. Grijpma, P.J. Dijkstra, R. Wang, Enzymatic post-crosslinking of printed hydrogels of methacrylated gelatin and tyramine-conjugated 8-arm poly(ethylene glycol) to prepare interpenetrating 3D network structures, Int. J. Bioprint. 9 (5) (2023) 522–537.
[58] G. Chakrapani, M. Zare, S. Ramakrishna, Intelligent hydrogels and their biomedical applications, Mater. Adv. 3 (21) (2022) 7757–7772.
[59] M.S. Yilmaz, E. Sahin, R. Kaymaz, B.Z. Altunkaynak, A.O. Akidil, S. Yanar, D. Demir, M. Guven, Histological study of the healing of traumatic tympanic membrane perforation after vivosorb and epifilm application, ENT-Ear Nose Throat 100 (2) (2019) 90–96.
[60] E. Sainsbury, R.D. Amaral, A.W. Blayney, R.M. Walsh, F.J. O'Brien, C. O'Leary, Tissue engineering and regenerative medicine strategies for the repair of tympanic membrane perforations, Biomater. Biosyst. 6 (2022) 100046–100055.
[61] J. Peng, H. Zhao, C. Tu, Z. Xu, L. Ye, L. Zhao, Z. Gu, D. Zhao, J. Zhang, Z. Feng, In situ hydrogel dressing loaded with heparin and basic fibroblast growth factor for accelerating wound healing in rat, Mater. Sci. Eng. C 116 (2020) 111169–111180.
[62] X. Zhang, X. Kang, L. Ji, J. Bai, W. Liu, Z. Wang, Stimulation of wound healing using bioinspired hydrogels with basic fibroblast growth factor (bFGF), Int. J. Nanomedicine 13 (2018) 3897–3906.